Journal of Alloys and Compounds 586 (2014) S189–S193

Contents lists available at SciVerse ScienceDirect

Journal of Alloys and Compounds

journal homepage: www.elsevier.com/locate/jalcom

Atomic structure and magnetic properties of Fe–Nb–B metallic glasses

I. Kaban [a,*], P. Jóvári [b], A. Waske [a], M. Stoica [a], J. Bednarčik [c], B. Beuneu [d], N. Mattern [a], J. Eckert [a,e]

[a] IFW Dresden, Institute for Complex Materials, P.O. Box 270116, D-01171 Dresden, Germany
[b] Wigner Research Centre for Physics, Institute for Solid State Physics and Optics, P.O. Box 49, 1525 Budapest, Hungary
[c] Deutsches Elektronen Synchrotron (DESY), Notkestrasse 85, D-22603 Hamburg, Germany
[d] Laboratoire Léon Brillouin, CEA-Saclay, 91191 Gif sur Yvette Cedex, France
[e] TU Dresden, Institute of Materials Science, D-01062 Dresden, Germany

ARTICLE INFO

Article history:
Available online 10 September 2012

Keywords:
Fe–Nb–B metallic glasses
Curie temperature
Atomic structure

ABSTRACT

The short-range atomic order of ternary Fe–Nb–B metallic glasses has been studied by X-ray diffraction, neutron diffraction, X-ray absorption spectroscopy, and reverse Monte-Carlo simulation. The similarities and differences in the local structure of the Fe–Nb–B glasses and their crystalline counterparts are revealed. The composition dependences for the Curie temperature of the Fe–Nb–B glasses, which increases by substitution of boron for iron at constant niobium content and decreases by substitution of niobium for iron at constant boron concentration, are discussed in the frame of the coordination-bond model.

1. Introduction

Fe–Nb–B alloys exhibit a good glass-forming ability (GFA); amorphous ribbons can be produced over a quite large composition range in the vicinity of the Fe corner on the concentration triangle [1]. Moreover, alloys with high boron content can form bulk metallic glasses [2,3]. GFA, thermal stability, mechanical and magnetic properties of the Fe–Nb–B glassy ribbons can be varied by adjusting the composition [1,4]. So far, Fe–Nb–B metallic glasses have been studied mainly due to their good soft magnetic and mechanical properties. Recently [5,6], attention has been paid to Fe–Nb–B amorphous and nanocrystalline alloys due to the magnetocaloric effect in which the temperature of a ferromagnetic material changes in an alternating external magnetic field [7,8]. The position of the maximum of the isothermal entropy change ΔS, which quantifies the magnetocaloric effect, approximately corresponds to the Curie temperature T_C. Therefore, for most magnetic refrigeration applications utilizing magnetocaloric effect, alloys with T_C close to room temperature are needed.

It is known that the Curie temperature of binary Fe–B amorphous alloys can be changed either by variation of the Fe:B ratio or by addition of a nonmagnetic element [9–15]. In this work, we show that the Curie temperature of Fe–Nb–B metallic glasses is systematically adjustable over a wide temperature range. We investigate the atomic structure of the Fe–Nb–B alloys by means of X-ray diffraction (XRD), neutron diffraction (ND) and extended X-ray absorption fine structure (EXAFS) measurements, as well as by the reverse Monte-Carlo (RMC) simulation technique.

2. Material and methods

2.1. Sample preparation

$Fe_{90-x}Nb_{10}B_x$ (x = 10, 20, 30 at.%) and $Fe_{71}Nb_6B_{23}$ master alloys were prepared by arc-melting of high purity Fe (99.95%), Nb (99.9%), and B (99.9% purity, from which 98.84% is ^{11}B) under a Ti-gettered Ar atmosphere. The ingots were re-melted in a quartz tube and rapidly quenched by single-roller melt-spinning on a copper wheel under Ar flow at 24 m s^{-1} tangential wheel velocity. By this, ribbons of about 20 μm thickness and 4 mm width were obtained.

2.2. Measurements

The mass density of the Fe–Nb–B melt-spun ribbons was determined by the Archimedean method using a computer controlled microbalance and dodecane as a working liquid. The estimated relative error of the mass density averaged over 50 measurements for each sample is about 0.5%.

Magnetic measurements were performed using a SQUID magnetometer (Superconducting Quantum Interference Device, Quantum Design) at magnetic field of 50 Oe. The instrument was equipped with a furnace enabling heating of the samples in borosilicate glass capillaries (1 mm inner diameter) up to 600 K. The Curie temperature was determined at the inflection point on the temperature-dependent magnetization curves with the accuracy of about ±2 K.

High-energy XRD measurements were performed in transmission geometry at the BW5 beamline at HASYLAB (DESY, Hamburg, Germany). The energy of the monochromatic synchrotron radiation was 100.0 keV and the cross section of the incident beam was 1 × 1 mm^2. Scattered X-ray photons were collected during 20 s using a MAR345 image plate detector mounted orthogonally to the incident beam. A LaB_6 standard was used to calibrate the sample-to-detector distance and to tilt the image plate relative to the beam path. The background intensity was

* Corresponding author. Tel.: +49 351 4659252; fax: +49 351 4659452.
E-mail address: i.kaban@ifw-dresden.de (I. Kaban).

0925-8388/$ - see front matter © 2012 Elsevier B.V. All rights reserved.
http://dx.doi.org/10.1016/j.jallcom.2012.09.008

Table 1
Mass and number density of the Fe–Nb–B melt-spun alloys.

Alloy	Mass density (g cm^{-3})	Number density (atoms Å^{-3})
$Fe_{80}Nb_{10}B_{10}$	7.80 ± 0.04	0.0853
$Fe_{70}Nb_{10}B_{20}$	7.56 ± 0.04	0.0900
$Fe_{71}Nb_6B_{23}$	7.45 ± 0.04	0.0940
$Fe_{60}Nb_{10}B_{30}$	7.30 ± 0.04	0.0955

subtracted directly from the two-dimensional XRD patterns and the result was integrated to the *Q*-space using the software package FIT2D [16]. The total X-ray structure factor *S*(*Q*) was calculated using standard procedures described in [17,18].

The neutron diffraction measurements were carried out with the 7C2 diffractometer at the Léon Brillouin Laboratory (CEA-Saclay, France). The wavelength of the incident radiation was 0.73 Å. Pieces of amorphous ribbons were placed into a thin-walled (0.1 mm) vanadium container of 7 mm diameter. The raw data were corrected for the detector efficiency and background scattering. Attenuation due to the sample absorption was estimated according to [19].

The EXAFS measurements at the Nb K-absorption edge were carried out at the beamline X1 (HASYLAB). The spectra were collected in transmission mode using fixed exit double-crystal Si(311). The intensities before and after the sample as well as after the reference sample were recorded by three ionisation chambers (IOC) filled with proper quantities of Ar, N_2, Kr, or their mixtures, to provide ~10% absorption in the first IOC, ~50% absorption in the second IOC, and ~75% absorption in the third IOC. The X-ray absorption cross sections $\mu(E)$ were converted to $\chi(k)$ by standard procedures of data reduction using the program VIPER [20].

2.3. Reverse Monte-Carlo modelling

Details on the reverse Monte-Carlo simulation method can be found in Refs. [21–23]. The rmc++ code [23] has been used for the modelling in the present work. The configuration box contained 25000 atoms in each case. The number densities used in the simulations of ternary Fe–Nb–B alloys were calculated from the experimental mass densities (Table 1). The number density of the $Fe_{80}B_{20}$ binary glass (0.0940 Å^{-1}) was obtained from the mass density (7.31 g/cm^3) reported in Ref. [24]. The accuracy of the partial coordination numbers N_{ij} and the mean interatomic distances r_{ij} for the Fe–Fe, Fe–Nb and Fe–B pairs is around 10% and ±0.02 Å, respectively. The error for the Nb–Nb and Nb–B pairs is around 25% (coordination numbers) and ±0.03 Å (interatomic distances).

3. Experimental results and RMC modelling

The experimental values of the mass density of the Fe–Nb–B melt-spun ribbons are listed in Table 1. The density of the $Fe_{90-x}Nb_{10}B_x$ (x = 10, 20, 30) alloys changes linearly with Fe concentration; it can be very well described by the function $d = [5.83 + 0.0246\ (90-x)]$ g/cm^3. The density of the $Fe_{71}Nb_6B_{23}$ composition is about 1.6% below an interpolated value for the $Fe_{71}Nb_{10}B_{19}$ density due to the substitution of boron for 4 at.% niobium.

The Curie temperature of the Fe–Nb–B metallic glasses measured in this work is presented together with the literature data [9–12] in Fig. 1. The Curie temperature significantly changes over a wide composition region (60–90 at.% Fe; 0–10 at.% Nb). At a fixed boron concentration, T_C increases linearly by about 23–25 K for every 1 at.% rise of the Fe concentration. At a fixed Nb concentration in the ternary Fe–Nb–B alloys, the Curie temperature increases with increasing B content in a similar manner as it has been reported for binary Fe–B metallic glasses [9–11].

The Faber–Ziman [25] total structure factors *S*(*Q*) obtained from the XRD intensities are shown in Fig. 2. The $Fe_{80}Nb_{10}B_{10}$ alloy was not completely amorphous, as it is seen from Fig. 2. The XRD scattering intensities and structure factors for the alloys with larger boron content did not show any crystalline peaks. Thus, the structure of these amorphous alloys was further studied.

The main problem in investigations of the local atomic order in the boron-poor alloys is the very small contribution of the boron-related atomic pairs to the experimental diffraction curves (see for example Table 2 for the XRD and ND weighting coefficients in the Fe–Nb–B alloys studied in this work). The total structure factors as

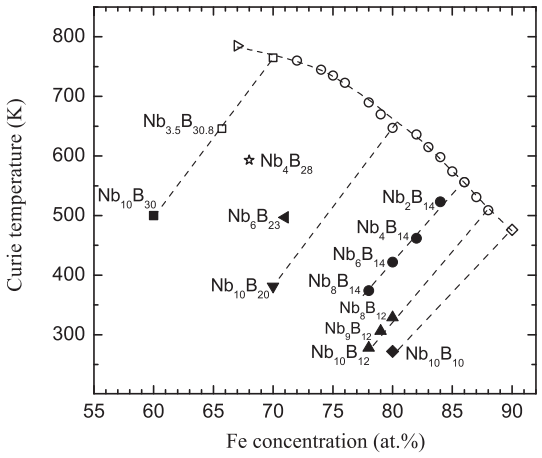

Fig. 1. Variation of the Curie temperature with composition of $Fe_{100-y-x}Nb_yB_x$ metallic glasses: *full symbols* – this work; *open symbols* – literature data [9–12]; *lines* are guides for the eye. Numbers on the figure give the concentration of Nb and B in ternary alloys.

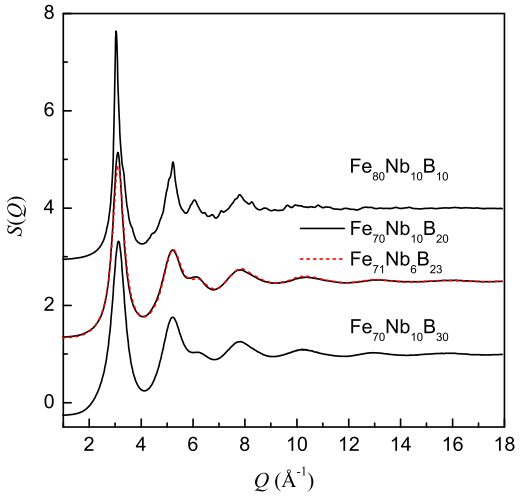

Fig. 2. XRD total structure factors for the melt-spun Fe–Nb–B alloys.

Table 2
XRD (at $Q = 0$) and ND weighting coefficients for the Fe–Nb–B alloys studied in this work. The values for ND are calculated for the case of ^{11}B isotope.

Pairs	$Fe_{70}Nb_{10}B_{20}$		$Fe_{71}Nb_6B_{23}$		$Fe_{60}Nb_{10}B_{30}$	
	XRD	ND	XRD	ND	XRD	ND
Fe–Fe	61.0	58.5	70.0	60.0	54.1	45.9
Fe–Nb	27.5	12.5	18.6	7.6	28.5	11.4
Fe–B	6.7	23.5	8.7	27.4	10.4	32.3
Nb–Nb	3.1	0.7	1.2	0.2	3.7	0.7
Nb–B	1.5	2.5	1.2	1.7	2.7	4.0
B–B	0.2	2.4	0.3	3.1	0.5	5.7

well as the corresponding pair distribution functions $g(r)$ for the Fe–Nb–B alloys mainly represent Fe–Fe, Fe–Nb and Fe–B pairs. The contribution of B–B and Nb–B pairs is negligibly small in the case of XRD. The situation is slightly better in the case of ND due to the use of the ^{11}B isotope. Nevertheless, the B–B, Nb–B, Nb–Fe and Nb–Nb contributions are hard to be resolved on the total pair distribution functions, as it is seen in Fig. 3.

It has been shown in a series of works (e.g., Refs. [26–29]) that the information on the local neighbourhood of certain atoms, missing in the XRD and ND data, can be obtained by EXAFS [30] if it

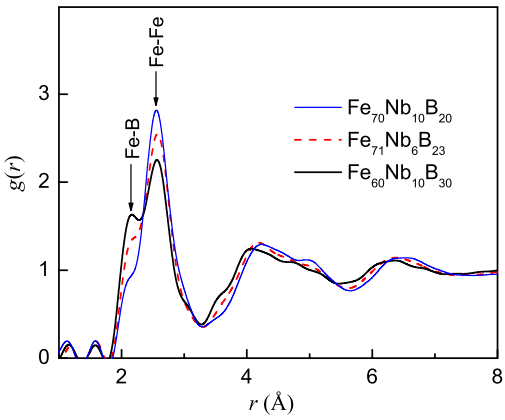

Fig. 3. ND total pair distribution functions for Fe–Nb–B metallic glasses. Nb–Fe, Nb–Nb, Nb–B and B–B contributions are hard to be resolved (see also text and Table 2).

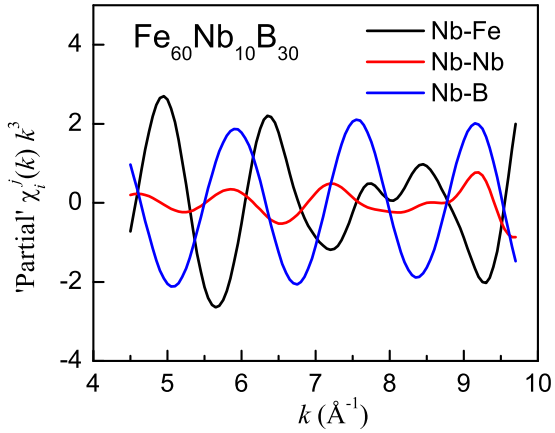

Fig. 4. Partial EXAFS Nb K-edge curves for the $Fe_{60}Nb_{10}B_{30}$ glass: the three $\chi_i^j(k)$-curves oscillate in different phase.

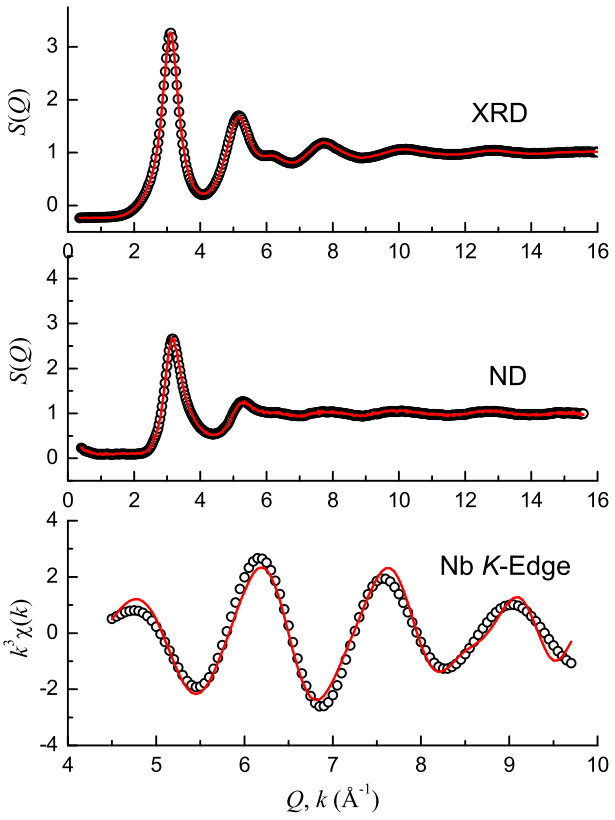

Fig. 5. RMC fits to the experimental XRD, ND and EXAFS curves for the $Fe_{60}Nb_{10}B_{30}$ glass: *circles* – experiment; *lines* – model. Boron–boron bonds were forbidden in the model.

resolves the environment of the absorbing atoms. For example, Fig. 4 shows the partial K-edge EXAFS curves for the $Fe_{60}Nb_{10}B_{30}$ alloy. All three curves oscillate in different phase, which suggests that the Nb–Nb, Nb–Fe, Nb–B pairs can be separated by analysis of the EXAFS data. At the moment, the reverse Monte-Carlo simulating technique seems to be the only tool enabling an effective combination of different experimental data such as XRD, ND, EXAFS by their simultaneous modelling. We have therefore applied the RMC technique in the present study of the Fe–Nb–B glasses.

Lamparter et al. [31] measured $Fe_{80}B_{20}$ glass by XRD and ND and calculated the partial coordination numbers and interatomic distances excluding B–B bonds. Pusztai and Sváb [26] applied RMC simulation to the $Ni_{65}B_{35}$ glass with rather high B content and found $N_{BB} \approx 1$, which was interpreted as a probable formation of short boron chains. Taking into account the relatively low boron content in the $Fe_{80}B_{20}$ alloy, we have modelled the experimental XRD and ND structure factors from the work [31] upon assumption that there are no B–B bonds. Due to the same reason, B–B bonds were forbidden in the RMC models of the $Fe_{70}Nb_{10}B_{20}$ and $Fe_{71}Nb_6B_{23}$ glasses. The structure of the $Fe_{60}Nb_{10}B_{30}$ composition was simulated both with and without B–B bonds. An excellent agreement of the experimental and simulated XRD and ND structure factors and a good agreement of the respective Nb K-edge EXAFS curves have been observed for both configurations. As an example, the RMC fits for the model without B–B bonds are shown in Fig. 5. The partial pair distribution functions obtained by the RMC modelling of the $Fe_{60}Nb_{10}B_{30}$ are shown in Fig. 6. Unfortunately, overlapping B–B and Fe–B $g_{ij}(r)$'s (Fig. 6a) do not allow to draw unambiguous conclusions about existence of boron-boron bonds in the $Fe_{60}Nb_{10}B_{30}$ metallic glass. We have also tested RMC models of the ternary Fe–Nb–B glasses with and without Nb–Nb bonds: the fits were slightly better if Nb–Nb bonds were allowed in the models. The mean bond lengths r_{ij}, partial coordination numbers N_{ij}, average number of neighbours of a given atomic species N_i, and total coordination numbers N extracted from the RMC models for all studied alloys are listed in Table 3.

4. Discussion

4.1. Local atomic structure

The Fe–Fe and Fe–B mean interatomic distances for the $Fe_{80}B_{20}$ composition (r_{FeFe} = 2.55 Å, r_{FeB} = 2.14 Å) obtained in our RMC simulation are in agreement with the respective values reported in Refs. [31–33]. It is interesting to compare the short-range order (SRO) parameters of the $Fe_{70}Nb_{10}B_{20}$ and $Fe_{60}Nb_{10}B_{30}$ glasses obtained by us (Table 3) with the respective data from the work of Imafuku et al. [34] who studied $Fe_{90-x}Nb_{10}B_x$ (x = 10, 20, 30) glasses by anomalous X-ray scattering and described the structure of the $Fe_{70}Nb_{10}B_{20}$ and $Fe_{60}Nb_{10}B_{30}$ glasses as a random network of $(Fe,Nb)_6B$-like trigonal prisms. In such prisms, one boron atom is surrounded by six nearest neighbours situated at the vertexes (five Fe atoms and one Nb atom), and the Fe–Fe and Fe–Nb distances within the triangular bases and the vertical edges are remarkably different.

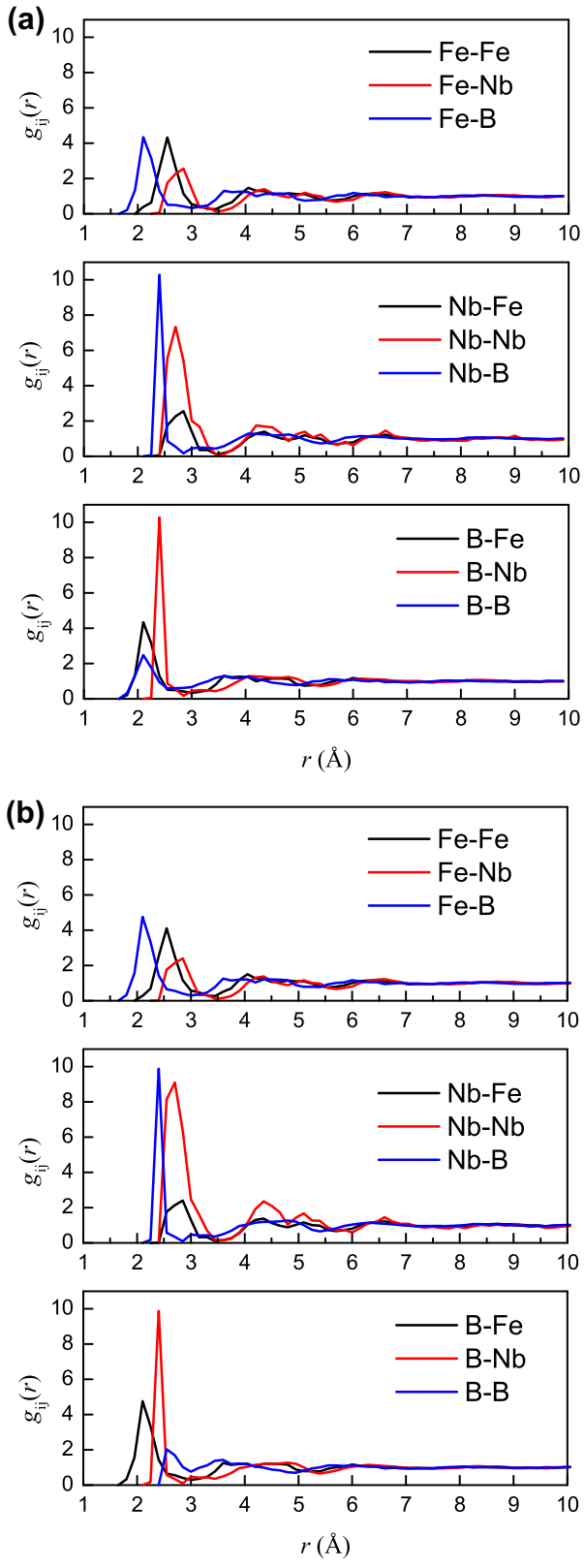

Fig. 6. Partial pair distribution functions for the $Fe_{60}Nb_{10}B_{30}$ glass obtained by the RMC simultaneous fitting experimental XRD, ND and EXAFS curves: (a) with boron–boron bonds; (b) without boron–boron bonds.

Partly, our results support the model of trigonal prism-like SRO in the $Fe_{70}Nb_{10}B_{20}$ and $Fe_{60}Nb_{10}B_{30}$ glasses – the mean interatomic distances obtained by the RMC simulations agree excellently with the first neighbour distances found by Imafuku et al. [34]. However, we did not observe any peak or shoulder on the Fe–Fe and Fe–Nb partial pair distribution functions around 2.84 and 3.33 Å, respectively, as reported in [34]. It is noteworthy that the Fe–Fe, Fe–Nb and Fe–B mean nearest neighbour distances in the ternary Fe–Nb–B glasses obtained by the RMC modelling fall into the middle of the respective bond lengths in crystalline $Fe_{69}Nb_{10.3}B_{20.7}$ ($Cr_{23}C_6$ structure) [35,36]: 2.432–2.664 Å for Fe–Fe, 2.454–2.946 Å for Fe–Nb, 2.127–2.145 Å for Fe–B. The Nb–B distance in the RMC models of the studied Fe–Nb–B glasses (2.40 Å) is significantly shorter than the Nb–B bond in the $Fe_{69}Nb_{10.3}B_{20.7}$ crystal (2.953 Å) [35,36]. The strengthening of the Nb–B bond can be explained by a high chemical affinity between Nb and B atoms (for example, the mixing enthalpy $\Delta H_{FeB} = -16$ kJ/mol, $\Delta H_{NbB} = -39$ kJ/mol [34]). The observed improvement of the RMC fits upon decreasing the Nb–Nb cut-off suggests that these bonds may be formed in the ternary Fe–Nb–B glasses. In general, our findings show that there are obvious similarities and differences in the short-range atomic order of the amorphous Fe–Nb–B glasses and related crystalline structures. Binary $Fe_{80}B_{20}$ and ternary Fe–Nb–B metallic glasses are characterised by dense atomic packing with a mean coordination number N of about 12.6 (Table 3). The mean coordination numbers for each component are quite large: $N_{Fe} = 13.8 \pm 1.4$, $N_{Nb} = 14.6 \pm 2.9$, $N_B = 8.5 \pm 1.7$ (the values are averaged over all compositions studied). The local atomic packing in the glassy state is more compact due to adjusting of the interatomic distances and probably due to formation of atomic bonds which do not exist in the crystalline state. These features might be responsible for the glass formation in the alloys studied.

4.2. Magnetic properties

In the frame of a mean-field model the absolute value of the Curie temperature of a glass containing transition metal(s) (TM) can be expressed as follows [37]:

$$T_c = J(r_{TM\text{-}TM}) N_{TM\text{-}TM} S(S+1)/3k_B \quad (1)$$

where $J(r_{TM\text{-}TM})$ is the distance-dependent interatomic exchange integral, $N_{TM\text{-}TM}$ is the TM–TM coordination number, S is the atomic spin quantum number, and k_B is the Boltzmann constant. Hence, principally, the Curie temperature can be changed with the composition of the glass by variation of the number of TM–TM nearest neighbours and/or distances. Both effects have been taken into consideration for the explanation of the non-monotonic composition dependence of T_C in binary Fe–B glasses (Fig. 1). O'Handley [37] suggested that (i) in the Fe-rich glasses (up to about 28 at.% boron) T_C increases with increasing boron concentration due to the increasing Fe–Fe distance r_{FeFe}, which causes a rise of the Fe–Fe exchange; (ii) upon further increase of the boron content, T_C decreases due to the increasing Fe–Fe distance, weakening the exchange, and due to decreasing coordination number of the magnetic species, N_{FeFe}.

Experimental and theoretical structural studies show a decrease of the Fe–Fe interatomic distance by increasing boron concentration in the Fe-rich Fe–B metallic glasses. For example, an increase of r_{FeFe} by about 0.016 Å between 16 and 23 at.% B has been established in the EXAFS study of Fdez–Gubieda et al. [32] and by about 0.04 Å between 9 and 36.3 at.% B in the molecular dynamics (MD) simulations of Tian et al. [33]. The Fe–Fe coordination number N_{FeFe} was suggested to be composition-independent in Ref. [32], while the MD study [33] showed that the Fe–Fe coordination number decreases with increasing boron concentration from 12.52 for $Fe_{91}B_9$ to 10.24 for $Fe_{63.7}B_{36.3}$.

The results of our RMC study of the $Fe_{90-x}Nb_{10}B_x$ melt spun ribbons (Table 3) reveal principally the same composition dependence for the Curie temperature and the Fe–Fe coordination number and distance as those found for the binary Fe–B glasses

Table 3
Bond lengths r_{ij} (Å), partial coordination numbers N_{ij}, average number of neighbours of a given atomic species N_i, and total coordination numbers N for the Fe–Nb–B glasses obtained by RMC modelling of the experimental XRD, ND and EXAFS data.

Pairs, *ij*	$Fe_{80}B_{20}$		$Fe_{70}Nb_{10}B_{20}$		$Fe_{71}Nb_6B_{23}$		$Fe_{60}Nb_{10}B_{30}$		$Fe_{60}Nb_{10}B_{30}$ *	
	r_{ij}	N_{ij}	r_{ij}	N_{ij}	r_{ij}	N_{ij}	r_{ij}	N_{ij}	r_{ij}	N_{ij}
Fe–Fe	2.55	11.70	2.52	10.21	2.55	10.76	2.56	9.55	2.56	9.63
Fe–Nb	–	–	2.79	1.52	2.81	0.81	2.78	1.18	2.78	1.25
Fe–B	2.15	1.82	2.11	1.72	2.13	2.25	2.15	3.56	2.15	3.23
Nb–Nb	–	–	2.70	1.38	2.83	1.51	2.71	3.96	2.71	3.13
Nb–B	–	–	2.40	2.46	2.40	4.03	2.40	3.48	2.40	3.78
B–B	–	0	–	0	–	0	–	0	2.13	1.79
N_{Fe}		13.52		13.45		13.82		14.29		14.11
N_{Nb}		–		14.47		15.09		14.55		14.40
N_B		7.28		7.25		10.08		8.28		9.51
N		12.27		12.31		13.04		12.51		12.76

* Boron–boron bonds were allowed in this RMC simulation.

in the works [9–11,32]. This suggests that the increase of the Fe–Fe interatomic distance and, respectively, of the exchange integral $J(r_{TM\text{-}TM})$ in Eq. (1) should prevail over the decrease of the Fe–Fe coordination number to explain the increase of the Curie temperature both in the Fe–B binary as well as in the Fe–Nb–B ternary metallic glasses with boron concentrations up to about 30 at.% at a constant Nb content. Obviously, the effect of decreasing N_{FeFe} becomes more significant by further increase of the boron concentration. The decrease of the Curie temperature upon the substitution of Nb for Fe can be explained by the simultaneous decrease of the Fe–Fe coordination number and interatomic distance; compare, for example, N_{FeFe} and r_{FeFe} in the $Fe_{80}B_{20}$ (11.70 and 2.55 Å) and in the $Fe_{70}Nb_{10}B_{20}$ (10.34 and 2.52 Å) or in the $Fe_{66.7}B_{33.3}$ [33] (10.58 and 2.58 Å) and $Fe_{60}Nb_{10}B_{30}$ glasses (9.55 and 2.56 Å), Table 3. The $Fe_{71}Nb_6B_{23}$ metallic glass with N_{FeFe} = 10.76 and r_{FeFe} = 2.55 (Table 3) follows the above tendency: for this composition T_C falls into the middle of a triangle between the Curie temperatures of the $Fe_{80}B_{20}$, $Fe_{70}Nb_{20}B_{20}$ and $Fe_{60}Nb_{10}B_{30}$ glasses (Fig. 1).

5. Conclusions

At constant niobium content, the Curie temperature of the Fe–Nb–B metallic glasses increases upon substituting iron by boron up to about 30 at.% boron. In this composition range, the increasing Fe–Fe interatomic distance is suggested to prevail over the decreasing Fe–Fe coordination number. In contrast, the Curie temperature decreases if iron is replaced by niobium at constant boron concentration. This effect is attributed to the decreasing Fe–Fe distance and coordination number.

The Fe–Fe, Fe–Nb and Fe–B mean nearest neighbour distances in the ternary Fe–Nb–B glasses have been found to fall into the middle of the interatomic bond lengths of the crystalline $Fe_{69}Nb_{10.3}B_{20.7}$ ($Cr_{23}C_6$ structure), while the Nb–B distance in the glassy state is significantly shorter than the respective bond in the $Fe_{69}Nb_{10.3}B_{20.7}$ crystal. Nb–Nb bonding, absent in the crystalline state, may exist in the ternary Fe–Nb–B glasses. These features could be responsible for the glass formation in the alloys studied.

Acknowledgments

This study has been partially supported by the German Research Foundation (Grant no. STO 873/2-1). P. Jóvári was supported by the OTKA (Hungarian Basic Research Found) Grant. no 083529. L. Pusztai is acknowledged for the help with neutron diffraction measurements. H. Hermann and R. Mazzarello are thanked for helpful discussions.

References

[1] S.T. Lin, C.L. Lee, J. Mater. Sci. 23 (1988) 1228–1324.
[2] M. Stoica, K. Hajlaoui, A. LeMoulec, A.R. Yavari, Philos. Mag. Lett. 86 (2006) 267–275.
[3] M. Stoica, K. Hajlaoui, J. Das, J. Eckert, A.R. Yavari, Rev. Adv. Mater. Sci. 18 (2008) 61–65.
[4] Z. Stokłosa, J. Rasek, P. Kwapuliński, G. Haneczok, A. Chrobak, J. Lelątko, L. Pająk, Phys. Status Solidi A 207 (2010) 452–456.
[5] I. Škovrănek, J. Kovač, Czech J. Phys. 54 (Suppl. D) (2004) D189–D192.
[6] J.J. Ipus, J.S. Blázquez, V. Franco, A. Conde, L.F. Kiss, J. Appl. Phys. 105 (2009) 123922 (6 pages).
[7] F. Bitter, Phys. Rev. 38 (1931) 528–548.
[8] E. Brück, in: K.H.J. Buschow (Ed.), Handbook of Magnetic Materials, vol. 17, North Holland, Elsevier, Amsterdam, 2008, pp. 235–291.
[9] R. Hasegawa, R. Ray, J. Appl. Phys. 49 (1978) 4174–4179.
[10] C.L. Chien, K.M. Unruh, Phys. Rev. B 24 (1981) 1556–1558.
[11] T. Nakajima, E. Kita, H. Ino, J. Mater. Sci. 23 (1988) 1279–1288.
[12] A.R. Yavari, G. Fish, S.K. Das, L.A. Davis, Mater. Sci. Eng. A (1994) 1415–1418.
[13] Y. Wan, X. Bi, Appl. Phys. Lett. 95 (2009) 262501 (3 pages).
[14] N. Hassanain, H. Lassri, R. Krishnan, A. Berrada, J. Magn. Magn. Mater. 146 (1995) 37–41.
[15] J. Torrens-Serra, P. Bruna, S. Roth, J. Rodriguez-Viejo, M.T. Clavaguera-Mora, J. Phys. D Appl. Phys. 42 (2009) 095010 (9 pages).
[16] A.P. Hammersley, S.O. Svensson, M. Hanfland, A.N. Fitch, D. Häusermann, High Pressure Res. 14 (1996) 235–248.
[17] H.F. Poulsen, J. Neuefeind, H.-B. Neumann, J.R. Schneider, M.D. Zeidler, J. Non-Cryst. Solids 188 (1995) 63–74.
[18] T. Egami, S.J.L. Billinge, Underneath the Bragg Peaks: structural analysis of complex materials, Pergamon Press, Elsevier, Oxford, England, 2003.
[19] H.H. Paalman, C.J. Pings, J. Appl. Phys. 33 (1962) 2635–2639.
[20] K.V. Klementev, J. Phys. D Appl. Phys. 34 (2001) 209–217.
[21] R.L. McGreevy, L. Pusztai, Mol. Simul. 1 (1988) 359–367.
[22] G. Evrard, L. Pusztai, J. Phys.: Condens. Matter 17 (2005) S1–S13.
[23] O. Gereben, P. Jóvári, L. Temleitner, L. Pusztai, J. Optoelectron. Adv. Mater. 9 (2007) 3021–3027.
[24] Y. Waseda, H.S. Chen, Phys. Status Solidi A 49 (1978) 387–392.
[25] T.E. Faber, J.M. Ziman, Philos. Mag. 11 (1965) 153–173.
[26] L. Pusztai, E. Sváb, J. Phys.: Condens. Matter 5 (1993) 8815–8828.
[27] I. Kaban, P. Jóvári, M. Stoica, J. Eckert, W. Hoyer, B. Beuneu, Phys. Rev. B 79 (2009) 212201 (4 pages).
[28] I. Kaban, P. Jóvári, T. Petkova, P. Petkov, A. Stoilova, B. Beuneu, W. Hoyer, N. Mattern, J. Eckert, in: J.P. Reithmaier, P. Paunovic, W. Kulisch, C. Popov, P. Petkov (Eds.), Nanotechnological basis for advanced sensors, NATO science for peace and security series b: physics and biophysics, Springer Netherlands, Dordrecht, 2011, pp. 195–202, http://dx.doi.org/10.1007/978-94-007-0903-4.
[29] I. Kaban, P. Jóvári, B. Bureau, M. Stoica, N. Mattern, J. Eckert, W. Hoyer, B. Beuneu, J. Phys.: Condens. Matter 22 (2010) 404208 (5 pages).
[30] J.J. Rehr, R.C. Albers, Rev. Mod. Phys. 72 (2000) 621–654.
[31] P. Lamparter, E. Nold, G. Rainer-Harbach, E. Grallath, S. Steeb, Z. Naturf. A 36 (1981) 165–172.
[32] M.L. Fdez-Gubieda, A. García-Arribas, J.M. Barandiarán, R. López Antón, I. Orue, P. Gorria, S. Pizzini, A. Fontaine, Phys. Rev. B 62 (2000) 5746–5750.
[33] H. Tian, C. Zhang, J. Zhao, C. Dong, B. Wen, Q. Wang, Physica B 407 (2012) 250–257.
[34] M. Imafuku, S. Sato, E. Matsubara, A. Inoue, J. Non-Cryst. Solids 312–314 (2002) 589–593.
[35] A. Takeuchi, K. Yubuta, A. Inoue, J. Phys.: Conf. Ser. 144 (2009) 012045. 5 pages.
[36] FIZ Karlsruhe ICSD, Coll. code 164057; http://www.fiz-karlsruhe.de/icsd.html.
[37] R. O'Handley, J. Appl. Phys. 62 (1987) R15–R49.